Metals and Materials International (2018) 24:525–531
https://doi.org/10.1007/s12540-018-0041-7

Isothermal Treatment Effects on Precipitates and Tensile Properties of an HSLA Steel

J.-E. Kim[1] · J.-B. Seol[2] · W.-M. Choi[1] · B.-J. Lee[1] · C.-G. Park[1,2]

Received: 30 June 2017 / Accepted: 12 September 2017 / Published online: 21 March 2018

Abstract
The relationships between tensile properties and precipitates of a high-strength low-alloy steel depending on the isothermal conditions were investigated. While the isothermally treated steel at 300–500 °C for 1 and 24 h had no significant difference, the steel treated at 500 for 336 h, denoted as 500–336 h, not only showed a decrease in tensile stress but also exhibited a highly increased elongation. Transmission electron microscopy and atom probe tomography were utilized to evaluate the precipitates distribution. The results showed that, in the case of 500–336 h sample, the fraction of precipitates with a radius over 10 nm is the highest and that of a few nano-sized precipitates is the lowest among all samples. It can be explained that the coarsening of originally nano-sized precipitates, occurred by diffusion of dissolved carbon in 500–336 h, mainly affects the tensile behavior.

Keywords Metals · Rolling · Precipitation · Tensile test · Transmission electron microscopy (TEM)

1 Introduction

Recently, high-strength low-alloy (HSLA) steels have been used in automotive components to obtain high strength caused by the combined effects of grain refinement and precipitation strengthening [1–4]. In addition to the strength, high ductility is also an essential property for automotive parts to achieve excellent formability [5]. It is well-established that the ferrite phase has high ductility and simultaneously low strength [6]. Therefore, during hot rolling process of HSLA steels, the step of austenite-to-ferrite transformation results in the high ductility through the formation of single phase ferrite matrix as well as the high strength through interphase precipitation of nano-sized carbides [1, 7]. Among alloying elements, Ti has a high affinity to carbon and forms carbides, thereby increasing the strength and hardness of steels by precipitation strengthening in conjunction with Mo, Nb and V [1, 5, 7–9]. In order to combine the high strength and ductility, precipitation of the nano-sized carbides in ferrite matrix is a suitable approach by hot rolling process. However, behavior of these carbides during isothermal treatment is not well known, although Yan et al. [10]. reported that the tensile properties are influenced by the strain-hardening exponents depending on the tempering temperature of lower bainitic HSLA steel.

Therefore, the purpose of this study is to investigate the relationship between the tensile properties and precipitates behaviors such as size and distribution of precipitates depending on the various isothermal conditions under the single phase state of ferrite.

2 Experimental

To analyse the effect of isothermal treatment, a low carbon steel containing alloying elements such as Ti, Mo, V and Nb was used as starting material (Table 1). The used HSLA steel experienced austenitization at 1250 °C in order to dissolve the solute elements, followed by a two-step hot rolling process at 920 °C and, subsequently, cooling to 640 °C of coiling temperature at cooling rate of 25 °C/s. Samples for analysis were cut off at the center position along the rolling direction of the fabricated plate. Isothermal heat treatments were conducted in a furnace under air atmosphere at 300 and 400 °C for 1

✉ C.-G. Park
cgpark@postech.ac.kr

[1] Department of Materials Science and Engineering, POSTECH, Pohang 34673, Republic of Korea

[2] National Institute for Nanomaterials Technology, POSTECH, Pohang 34673, Republic of Korea

Table 1 Chemical composition of the used HSLA steel (unit: wt%)

C	Mo	Ti	V	Si	Mn	Al	Nb	Fe
0.08	0.25	0.14	0.1	0.2	1.3	0.03	0.02	Bal.

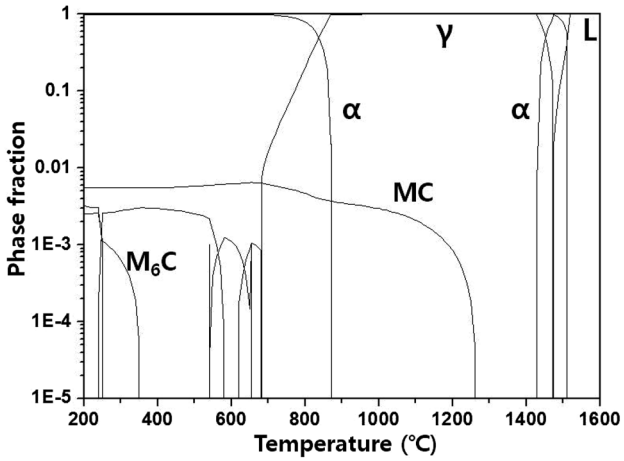

Fig. 1 Thermodynamic simulation of phase fraction for the used HSLA steel by Thermocalc

and 24 h, respectively denoted as 300–1, 300–24, 400–1 and 400–24 h, and 500 °C for 1, 24 and 336 h, likewise denoted as 500–1, 500–24 and 500–336 h. As shown in Fig. 1, the starting and finishing temperature of phase transformation from austenite to ferrite during cooling is about 870 and 680 °C. It can be predicted that phase transformation and interphase precipitation of MC type carbides mainly such as (Ti, Mo, V) C and few M6C type carbides such as (Ti, Mo, V)6 C occur during cooling after two-steps hot rolling process. To identify the interphase precipitates of as rolled sample, analysis of transmission electron microscopy (TEM) was performed using Cs corrected STEM (Scanning TEM, JEOL, JEM-2100F) with high-angle annular dark field (HAADF) imaging. Specimens for TEM observations were prepared by lift out method using a dual beam focused ion beam (FIB) (FEI, Helios Nano-Lab 600) equipment.

Specimens for tensile tests were fabricated along rolling direction with a gauge length of 6.39 mm and a thickness of 1 mm. The stress and ductility were tested at a strain rate of 10^{-3} mm/s at room temperature using Instron machine. For reproducibility, more than two specimens per each condition were tested.

Electron backscatter diffraction (EBSD) installed on FIB was used to compare the average grain size and phase fraction under an acceleration voltage of 20 kV and a beam current of 22 nA with a step size of 0.2 μm. For the EBSD analysis, the surface of samples was ground down to 0.25 μm and etched by a solution of 5% perchloric acid.

To identify the distribution and size of the precipitates, a two-step analysis were performed: (1) TEM analysis by replica method, (2) APT analysis. For TEM analysis, the surface of sample was etched using a solution of 5% nital following the mechanically polishing to 0.25 μm. After coating of carbon and removing the carbon layer in a solution of 10% nital, the extracted replicas were placed on the Cu grid.

For APT analysis, needle-shaped specimens were fabricated by a dual beam FIB. By an annular milling process, the sharpening for the needle-shaped specimens was performed using Ga^+ ion beam and the final specimen with a tip radius of ~ 50 nm was loaded into the atom probe. APT measurements using a local electrode atom probe (LEAP; CAMECA, LEAP 4000X HR) were performed in laser mode at a temperature of 50 K with a pulse energy of 100 pJ and a pulse rate of 200 kHz. The reconstructions and cluster analyses of APT results were done using the IVAS software (3.6.10a version) by CAMECA Instruments. The reconstructions were calibrated by shank angle of needle-shaped specimens. To investigate the precipitates in the matrix, the maximum separation algorithm was employed [11].

3 Results and Discussion

3.1 Interphase Precipitation

TEM studies were carried out to identify the precipitation behavior of as-rolled sample formed during hot rolling process. Under the TEM observation, specimens must be tilted to confirm a planar array consisting of carbides as precipitates because interphase precipitation occurs along specific direction moving the austenite/ferrite boundaries [12, 13]. STEM-bright field (BF) image in Fig. 2a shows that the array of precipitates indicated as dashed line were formed along [110] direction with a layer spacing of 12–14 nm. To verify the orientation relationship between ferrite matrix and precipitates, results of HR-TEM and fast Fourier transformation (FFT) in Fig. 2b were considered. The precipitate has a length of 13 nm as the longest direction. The HR-TEM image and diffraction pattern obtained by FFT indicating precipitates and ferrite were satisfied to the Baker-Nutting orientation [14, 15]. During interphase precipitation, precipitates has specific orientation relationship such as $(001)_{PPT}$// $(001)_{\alpha}$ and $[110]_{PPT}$//$[100]_{\alpha}$ with respect to the ferrite matrix. Thus, it means that precipitates were formed at the boundaries of austenite/ferrite within a range of transformation temperature from austenite to ferrite after hot rolling process.

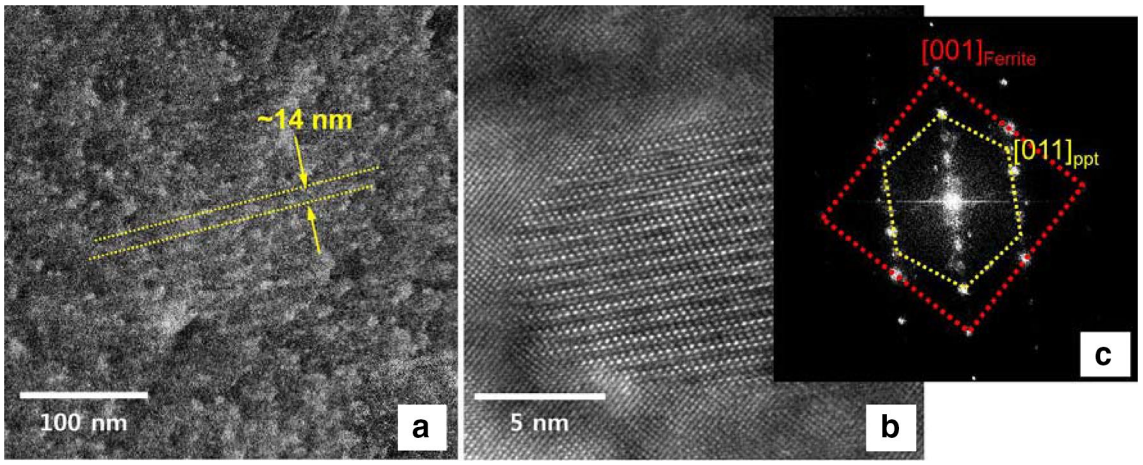

Fig. 2 **a** Microstructure of as-rolled sample showing interphase precipitates along [001] ferrite zone axis [7], **b**, **c** HR-image of precipitate and its fast Fourier transformation (FFT) [7]

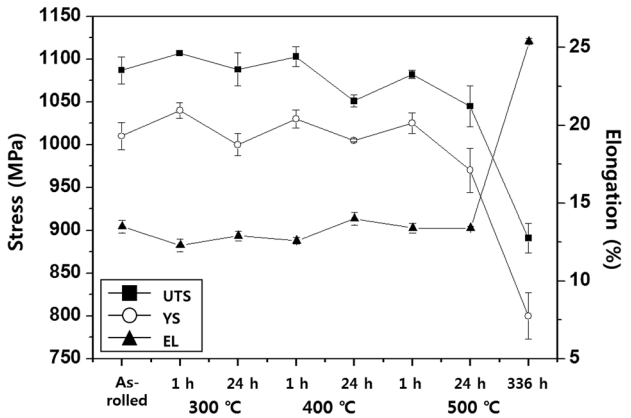

Fig. 3 Ultimate tensile stress (UTS) versus yield stress (YS) versus tensile strain depending on the isothermal treatment conditions

3.2 Tensile Properties and Microstructure

Figure 3 shows the values of tensile stress and elongation for all samples. As-rolled sample has a UTS of ~ 1130 MPa and a tensile strain of ~ 12%. With increasing the time or temperature of heat treatment, UTS decreases and tensile strain increases, but there was no great difference except for 500–336 h sample. For example, a maximum rates of UTS decrease and tensile strain increase for 500–24 h sample are ~ 7 and ~ 17% in comparison to as-rolled sample. However, as for 500–336 h sample, the values of UTS and tensile strain change to ~ 900 MPa and ~ 25%, respectively, representing 20% reduction in UTS and 108% increase for tensile strain with respect to the as-rolled sample. The results of yield stress (YS) have also a similar tendency with UTS and it will be discussed in following.

To understand these phenomena, we confirmed a microstructure using by EBSD. The microstructure of as-rolled sample versus 500–336 h sample and average grain size of all samples is presented in Fig. 4. Grain morphology and size between as-rolled sample and 500–336 h sample is not completely different shown in Fig. 4b, c. Average grain size of as-rolled steel, which is composed of ferrite single phase, is 4.0 μm. Although the average grain size increases to 4.8 μm with increasing the temperature and time of isothermal treatment (see Fig. 4c), the difference is very small. Moreover, ferrite is the only phase for all samples because isothermal treatment was performed in the temperature range of ferrite single phase area, as shown in Fig. 1. Therefore, it can be concluded that the main factor affecting the tensile properties of isothermally treated samples is not microstructures such as grain size and phase fraction but precipitates distribution depending on the isothermal treatment conditions.

3.3 Distribution of Precipitates

The precipitates were analysed by TEM and distribution of those with radius over 10 nm was identified as shown in Figs. 5 and 6. The distributions of precipitates of as-rolled sample and 500–336 h sample are clearly different in Fig. 5. The number density of precipitates in 500–336 sample is significantly higher and radius is smaller than in as-rolled sample. The calculated number density of precipitates decreases with increasing the temperature and time of isothermal treatment except for 500–336 h sample, as indicated in Fig. 6. Simultaneously, the average size of precipitates increases, even though the values for 300–1 and 400–1 or 300–24 h and 400–24 h samples has no great difference. However, in the case of 500–336 h, the average precipitates size decreases, although the number density of precipitates is the highest among all conditions of isothermal treatment.

Figure 7a, b present the 3D atom map of a few nano-sized precipitates of 500–24 and 500–336 h samples obtained by

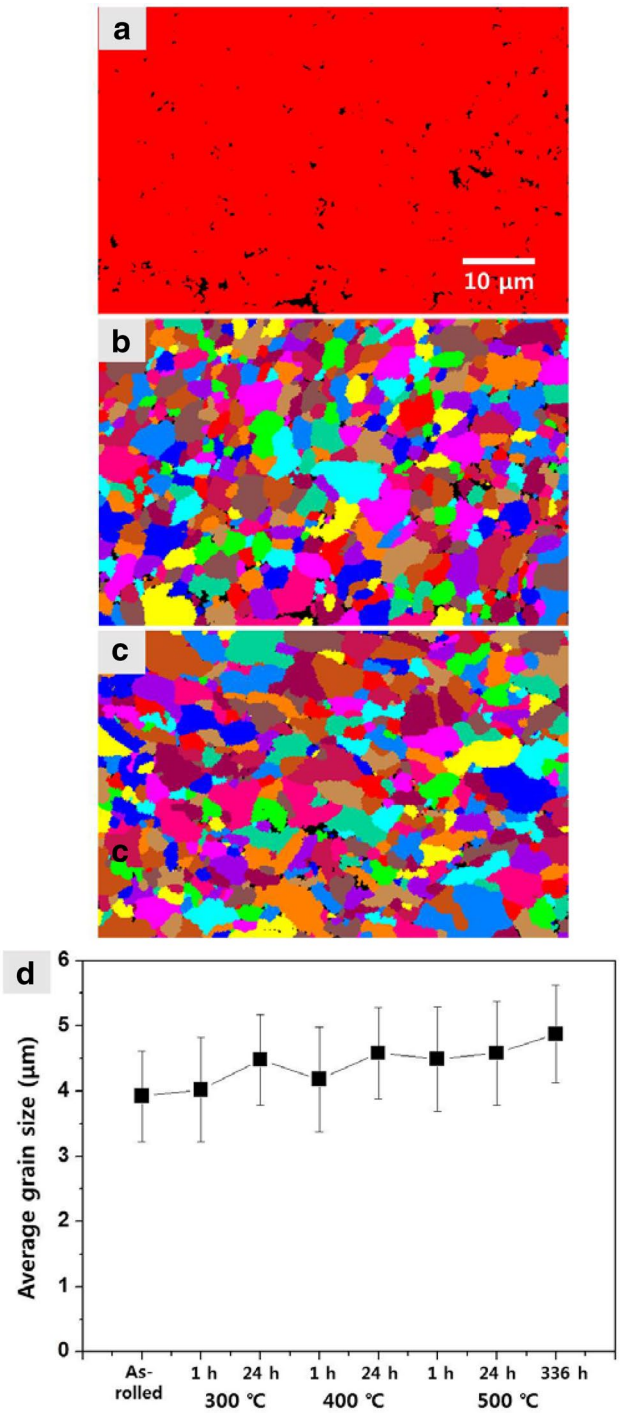

Fig. 4 **a** Phase map (red color represents ferrite phase), **b** grain map of as-rolled sample, **c** grain map of 500–336 h sample obtained by EBSD **d** average grain size depending on the isothermal treatment conditions. (Color figure online)

APT analysis. In contrast to the results obtained by TEM-replica analysis, the number density in 500–336 h sample is lower than one in 500–24 h. The number density of precipitates about all samples is calculated on the basis of 3D atom map. As a results, although other samples have the number density of ~ $2.0 \times 10^{24}/m^3$, only 500–336 h sample has that of ~ $1.0 \times 10^{24}/m^3$ as shown in Fig. 7c. It is suggested that the nano-sized precipitates were newly formed, whereas the coarsening of precipitates within as-rolled sample occurred during isothermal treatment by diffusion of dissolved C in the matrix. In addition, the fraction of precipitates with a radius over 10 nm is highly larger than one of nano-sized precipitates. By considerable increase of the coarsened precipitates fraction, the tensile stress decreases significantly to under 900 MPa, although the nano-sized precipitates, which affect the precipitation hardening in low carbon steel, act as obstacles for the existing dislocations glide [16–18]. Figure 7d shows the concentration profile of a few nano-sized precipitates investigated by APT. The composition of precipitates is $(Ti_{15}Mo_{15}V_{10})C_{30}$ and it is MC-type carbide even though content of C is not ideal stoichiometry of MC-type carbide due to vacancies of C. Besides, precipitates have core/shell structure with a Ti-V-C core and a Mo shell. Therefore, it can be concluded that these precipitates are stable during isothermal treatment because they are core/shell structure [7].

For dislocations movement, thermal activation energy and enough time are positively necessary [19]. Since the isothermally treated samples for 1 and 24 h in the range of 300–500 °C have not sufficient time and temperature, it is inferred that the density of dislocations has not changed significantly and the tensile stress is maintained at a value above 1000 MPa. However, since the movement of dislocations is active in 500–336 h sample, dislocations having the opposite Burgers vector encountered and disappeared [19]. Finally, the number of mobile dislocations and density of dislocations decrease and, furthermore, there is more sufficient space for dislocations gliding. Regarding that the tensile properties are associated with the density of dislocation, and this parameter decreases for 500–336 h sample, the tensile strain increases to ~ 25% and the ductility is eventually improved.

3.4 Strength Mechanism by Precipitates

Total yield stress of ferritic steel can be calculated by the following equation [20, 21]:

$$\Delta\sigma_y = \Delta\sigma_0 + \Delta\sigma_{SS} + \Delta\sigma_{GB} + \sqrt{\Delta\sigma_{Dis}^2 + \Delta\sigma_{Pre}^2} \quad (1)$$

where $\Delta\sigma_0$ is the friction stress of the ferritic matrix, $\Delta\sigma_{SS}$ is the increased yield stress due to solid solute strengthening, $\Delta\sigma_{GB}$ is the increased yield stress due to grain boundary strengthening $\Delta\sigma_{Dis}$, is the increased yield stress resulted from the dislocation strengthening and $\Delta\sigma_{Pre}$ is the increased yield stress due to precipitation strengthening. The sum of $\Delta\sigma_0$, $\Delta\sigma_{SS}$, $\Delta\sigma_{GB}$ and $\Delta\sigma_{Dis}$ calculated by Eq. (1) is

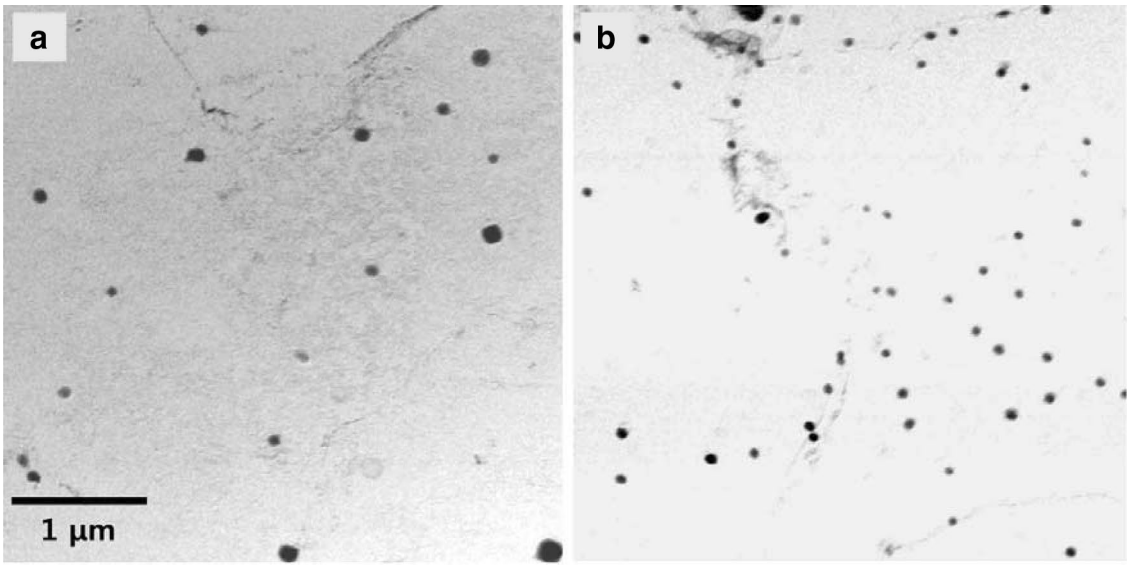

Fig. 5 TEM micrographs showing the distribution of precipitates of **a** as-rolled sample and **b** 500–336 h sample

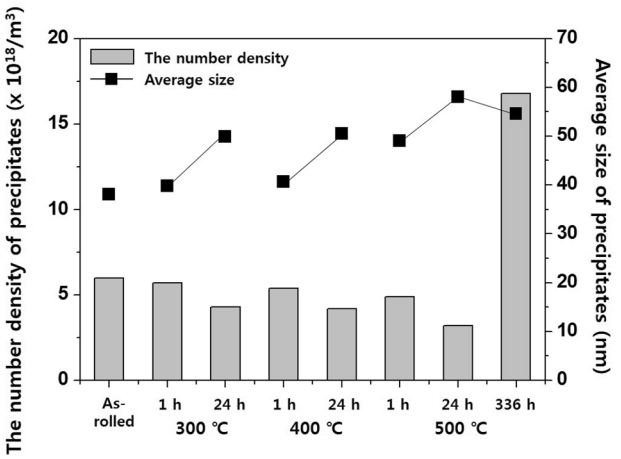

Fig. 6 The number density and average size of precipitates with a radius over 10 nm calculated by TEM analysis

~ 400 MPa. Therefore, among these factors, the increased yield stress resulted from precipitation strengthening ($\Delta\sigma_{Pre}$) is the most important factor contributing to total yield stress [1, 5, 12]. An amount of $\Delta\sigma_{Pre}$ is estimated by the following equation [22],

$$\Delta\sigma_{Pre} = \frac{K}{d} f^{1/2} \ln \frac{d}{b} \quad (2)$$

where K is a constant (5.9 N/m), b is Burger's vector (0.246 nm), f is a volume fraction of the precipitates and d is a diameter of precipitates. According to Eq. (2), calculated $\Delta\sigma_{Pre}$ of all samples except for 500–336 h sample is ~ 650 MPa, whereas that of 500–336 h sample is ~ 450 MPa. Although density of precipitates with a radius over 10 nm is the highest in sample of 500–336 h, the increased yield stress from precipitates strengthening is the lowest because not only the volume fraction of precipitates with a radius over 10 nm is very low as compared with that of a few nano-sized precipitates but also density of a few nano-sized precipitates by coarsening. As well as, it is also confirmed that the increased yield stress due to precipitates strengthening has a significant effect on the total yield stress of isothermally treated ferritic steels.

4 Conclusions

The effects of isothermal treatment on tensile properties of low carbon ferritic steel were investigated by EBSD, TEM and APT. The following results are obtained.

1. All isothermally treated samples has a ferrite single phase and grains with an average diameter of ~ 4.5 μm, because isothermal treatment was performed in temperature range of ferrite single phase area and the temperature did not reach to recrystallization temperature.
2. While the samples heat treated for 1 and 24 h in the temperature range of 300–500 °C showed no significant differences, tensile properties changed steeply in the case of 500–336 h sample. It is considered that tensile stress such as UTS and YS decrease as coarsening of a few nano-sized precipitates.
3. The calculated sum of the increased yield stress of $\Delta\sigma_0$, $\Delta\sigma_{SS}$, $\Delta\sigma_{GB}$ and $\Delta\sigma_{Dis}$ is ~ 400 MPa. In addition, except for 500–336 h sample, the calculated $\Delta\sigma_{Pre}$ of all sam-

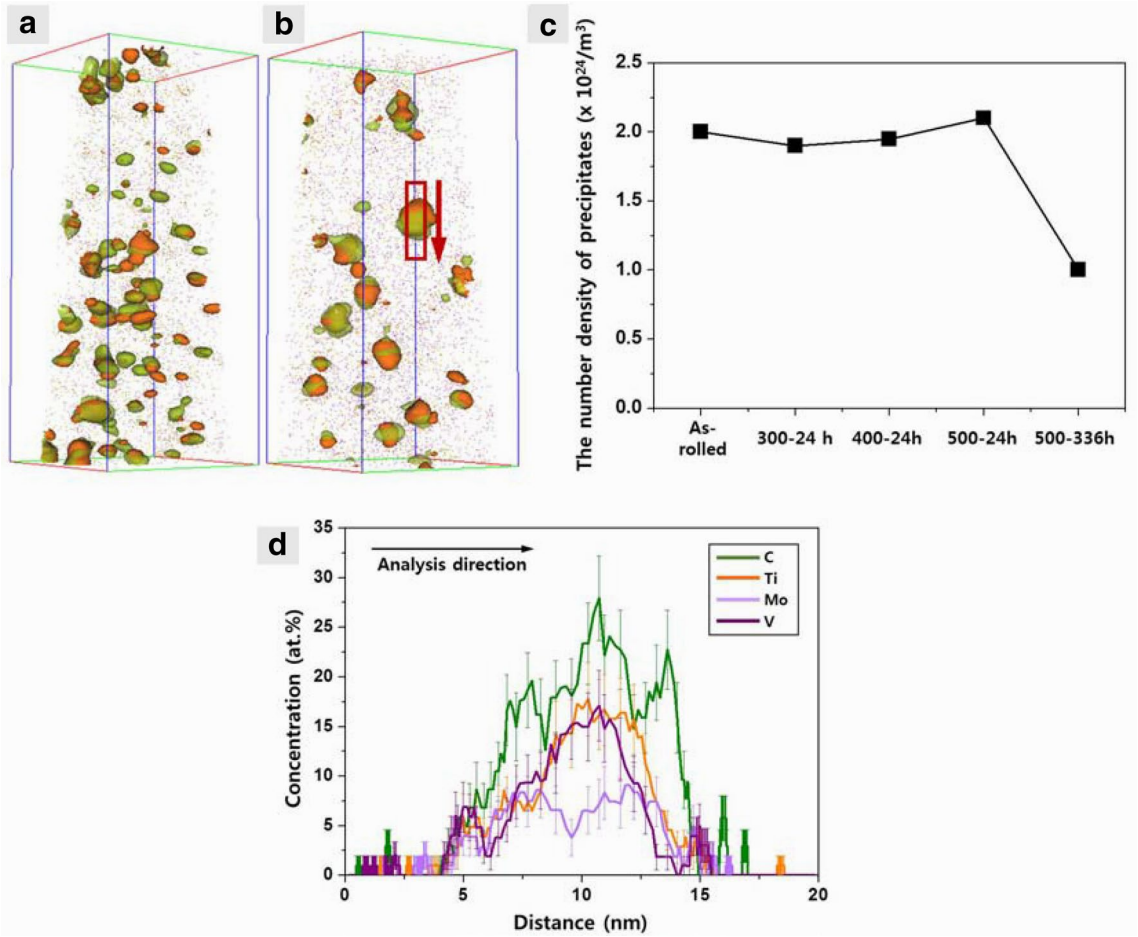

Fig. 7 The distribution of precipitates with a few nm radius in **a** 500–24 h and **b** 500–336 h samples, **c** the number density of precipitates with a radius of a few nm, **d** concentration profiles of precipitate analyzed by APT along the red arrow in the red square box in (**b**). (Color figure online)

ples is ~ 650 MPa while that of 500–336 h sample is ~ 450 MPa. These calculated results of the total yield stress are well matched with experimental results.

4. It is confirmed by calculating each factor that among various factors, $\Delta\sigma_{Pre}$ contributes to the total yield stress in these isothermally treated ferritic steels.

Acknowledgements The authors gratefully acknowledge the financial support from POSCO and the National Institute for Nanomaterials Technology (NINT), Korea.

References

1. Y. Funakawa, T. Shiozaki, K. Tomita, T. Yamamoto, E. Maeda, ISIJ Int. **44**(11), 1945 (2004)
2. K.B. Kang, O. Kwon, W.B. Lee, C.G. Park, Scr. Mater. **36**, 1303 (1997)
3. H. Ohtska, M. Umemoto, I. Tamura, in *Proceednigs of International Conference on Thermec*, vol 88, Tokyo, Japan (1988), p. 352
4. A. Bakkaloglu, Mater. Lett. **56**, 263 (2002)
5. X. Wang, A. Zhao, Z. Zhao, Y. Huang, Z. Geng, Y. Yu, J. Iron. Steel Res. Int. **21**(12), 1140 (2014)
6. T. Inoue, S. Kinoshita, J. Jpn. Technol. Plast. **14**(147), 291 (1973)
7. J.B. Seol, S.H. Na, B. Gault, J.E. Kim, J.C. Han, C.G. Park, D. Raabe, Sci. Rep. **7**, 42547 (2017). https://doi.org/10.1038/srep42547
8. X. Wang, H. Di, G. Wang, X. Liu, J. Iron. Steel Res. Int. **19**(6), 64 (2012)
9. Y. Shen, C. Wang, X. Sun, Mater. Sci. Eng. A **528**, 8150 (2011)
10. W. Yan, L. Zhu, W. Sha, Y. Shan, K. Yang, Mater. Sci. Eng. A **517**, 369 (2009)
11. J.M. Hyde, E.A. Marquis, K.B. Wilford, T.J. Williams, Ultramicroscopy **111**, 440 (2011)
12. H.W. Yen, P.Y. Chen, C.Y. Huang, J.R. Yang, Acta Mater. **59**, 6264 (2011)
13. H.W. Yen, C.Y. Huang, J.R. Yang, Adv. Mater. Res. **663**, 89 (2009)
14. M.Y. Chen, M. Goune, M. Verdier, Y. Brechet, J.R. Yang, Acta Mater. **64**, 78 (2014)

15. B.G. Baker, J. Nutting, J. Precipit, Process Steels Spec. Rep. **64**, 1 (1959)
16. Z.W. Zhang, C.T. Liu, Y.R. Wen, A. Hirata, S. Guo, G. Chen, M.W. Chen, B.A. Chin, Metall. Mater. Trans. A **43**, 351 (2012)
17. Z.W. Zhang, C.T. Liu, S. Guo, J.L. Cheng, G. Chen, T. Fujita, M.W. Chen, Y.W. Chung, S. Vaynman, M.E. Fine, B.A. Chin, Mater. Sci. Eng. A **528**, 855 (2011)
18. M.K. Miller, K.F. Russell, J. Nucl. Mater. **371**, 145 (2007)
19. W. Yan, L. Zhu, W. Sha, Y.Y. Shan, K. Yang, Mater. Sci. Eng. A **517**, 369 (2009)
20. F.B. Pickering, *Physical Metallurgy of Microalloyed Steel* (Applied Science Publishers, Londen, 1978), p. 63
21. A.J.E. Foreman, M.J. Makin, Can. J. Phys. **45**, 511 (1967)
22. N. Matsuzu, A. Itami, K. Koyama, SAE Technical Paper Series No. 910513